Organic & Biomolecular Chemistry

ROYAL SOCIETY OF CHEMISTRY

PAPER

View Article Online
View Journal | View Issue

Cite this: *Org. Biomol. Chem.*, 2021, **19**, 6858

Biological halogen bonds in protein–ligand complexes: a combined QTAIM and NCIPlot study in four representative cases†

Antonio Frontera * and Antonio Bauzá *

Received 23rd June 2021,
Accepted 19th July 2021

DOI: 10.1039/d1ob01212f

rsc.li/obc

In this study, the PDB has been manually scrutinized by using a subset of all PDB entries containing organic iodinated ligands. Four structures exhibiting short I···A halogen bonding (HaB) contacts (A stands for the σ-hole acceptor) have been selected and further analysed. In most hits, the sigma-hole acceptor corresponds to an O-atom of the amido group belonging to the protein backbone. In a minority of hits, the electron donors are O, S, Se or π-systems of the amino-acid side chains. A judicious selection of four PDB structures presenting all four types of HaB interactions (C–I···A, A = O, S, Se, π) has been performed. For these selected structures, a comprehensive RI-MP2/def2-TZVP study has been carried out to evaluate the HaB energetically. Moreover, the interactions have been characterized by combining the quantum theory of "atoms-in-molecules" (QTAIM) and the noncovalent interaction plot (NCIPlot) and rationalized using the molecular electrostatic potential (MEP) surface.

Introduction

In the last decade, σ-hole interactions are certainly emerging from the shadow of the ubiquitous H-bond.[1] Interactions involving groups 14–17 elements of the periodic table acting as electron acceptors are commonly used nowadays in crystal engineering and catalysis.[2–15] However, the hydrogen bond (HB) is still prevailing in the toolbox of supramolecular chemists and chemical engineers to design and control molecular assemblies in solution and in the solid state.[16] This fact is especially true in biology, where the HB is inescapably dominant, exemplified by the secondary structures of peptides and proteins and the function at all levels of proteins, nucleic acids and carbohydrates.[17] Moreover, the solvent that surrounds all these biopolymers is water, the prototypical HB donor/acceptor molecule.[18] Therefore, the HaB investigations in biological systems are not abundant and their utilization is not well-appreciated by the biological community. In fact, halogenation of biopolymers is related to several diseases, such as asthma or chronical inflammation.[19–24]

P. S. Ho's group has been actively involved in characterizing the prevalence, geometric constraints, and structure–function relationship of HaBs in biological systems.[25–29] P. S. Ho *et al.* have recently recommended a set of criteria for how to determine whether biological HaBs would have biological relevance.[30] These criteria are as follows: the HaB (1) should affect a biological function, (2) should affect the structures and stabilities of the biomolecules that define that function, and (3) have energies that are sufficiently large to be relevant in affecting biological structures and functions. Ho's group has proposed that for a HaB to be biologically relevant, it must contribute with a significant amount of energy, at least comparable to that of an HB.[30] Therefore, it is important to quantify the strength of biological HaBs in a reliable manner to ensure that they are biologically relevant. While many force fields are unable to quantify HaBs accurately,[31–34] quantum mechanics (QM) calculations can provide reliable estimations of their strength.[35,36] In this regard, besides the criteria proposed by Ho *et al.*,[30] it would be recommended that the existence of the biological HaB contact is further evidenced by using the Bader's quantum theory of "atoms-in-molecules" (QTAIM),[37] as it is explicitly stated in the definition of the halogen bond (IUPAC Recommendations 2013).[38]

In this manuscript we have examined the Protein Data Bank[39] (PDB) (*vide infra*) and four selected PDB structures exhibiting four types of HaBs with iodinated ligands. The strength of these biological HaB interactions has been estimated using RI-MP2 (resolution of the identity second order Moller–Plesset) calculations and theoretical models of the ligand and active sites. The I···A interactions (A = O, S, and Se and π-system) have been characterized by QTAIM and noncovalent interaction plot (NCIplot)[40] index surface analyses.

Departament de Química, Universitat de les Illes Balears, Crta. de Valldemossa km 7.5, 07122 Palma de Mallorca, Baleares, Spain. E-mail: toni.frontera@uib.es, antonio.bauza@uib.es

†Electronic supplementary information (ESI) available: PDB table and X-ray Cartesian coordinates of all optimized models. See DOI: 10.1039/d1ob01212f

Results and discussion

Preliminary PDB analysis

Fig. 1 shows the results of the manual inspection of the PDB where the only restriction was the presence of an organo-iodine derivative in the structure. From the total of proteins (660) present in the PDB having an organo-iodine as a complexed ligand, 20.2% are involved in halogen bonding interactions. Among these, the most frequent interaction (more than 90% of structures) is established with O-atoms of amido groups belonging to the protein backbone acting as electron donors.

More precisely, the carbonyl group of VAL residues is the most abundant electron donor moiety, followed by LEU and GLY carbonyl groups. In addition, the carbonyl group of PHE and the hydroxyl group of TYR residues are also involved as electron donor moieties. Furthermore, strong electron donor groups such as carboxylate moieties from ASP and GLU residues exhibit low abundance. Lastly, ARG, ILE, SER and GLN carbonyl groups are among the less abundant residues involved as electron donor partners (see Table S1 in the ESI† for more details).

It is also interesting to point out that when only considering O as an electron donor atom most hits exhibited C–I···O distances comprised between 3.0 and 3.50 angstroms (Fig. 2 top), which lies beneath the sum of the I and O vdW radii ($\sum R_{vdW}$ = 3.54 Å). In addition, the angle distribution including all the electron donor atoms (O, S, Se and C) shows the high directionality of the interaction, since most hits exhibit C–I···A (A = O, S, Se, C) angles gathered between 170 and 180 degrees (Fig. 2 bottom), as it has been observed in other crystallographic studies.[10]

These results are in line with previous and more comprehensive statistical PDB analyses,[29,41,42] which showed that the carbonyl O-atom of the peptide bond is the most common HaB acceptor, followed by other electron-rich acceptors (N, S, Se, and pi systems).[41] Previous surveys have also evidenced that biological HaBs with iodine in protein–ligand complexes present strong linearity.

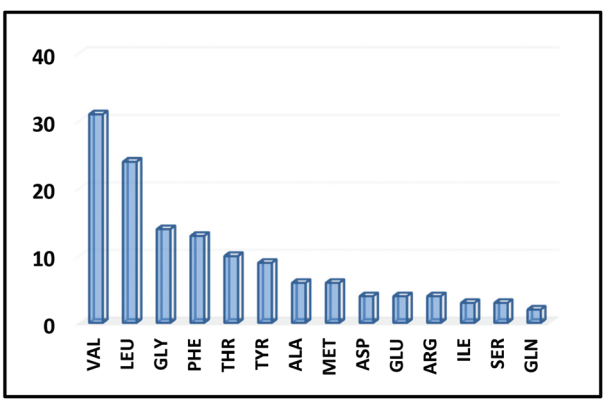

Fig. 1 Total count of PDB structures where each AA acts as an electron donor entity.

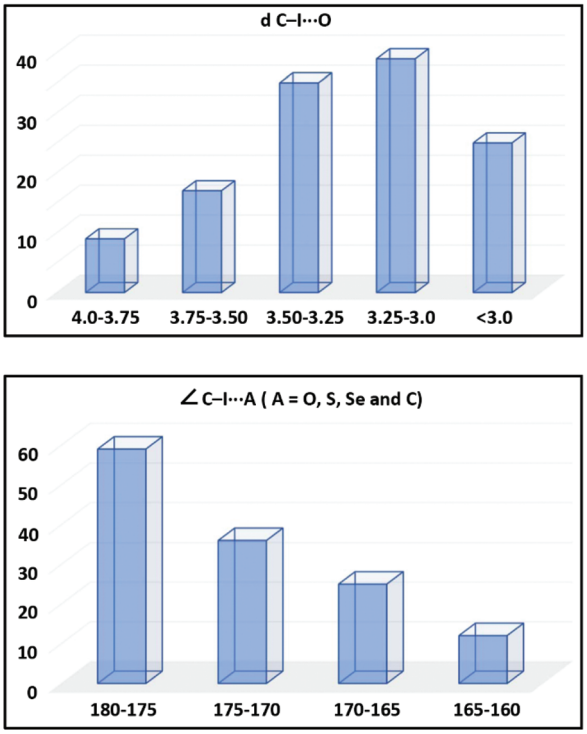

Fig. 2 Distance (top) and angle (bottom) distribution of HaBs in protein–ligand complexes.

Theoretical study on selected biological HaBs

The main purpose of the previous PDB analysis was the selection of several hits to be studied theoretically. Therefore, using a reduced set of hits with C–I···A angles close to linearity and short I···A distances, the final selection of four hits was based on: (i) structures high resolution (low crystallographic *R*-value) and (ii) a representation all the four types of HaB interactions observed during the manual inspection of the structures that depend on the nature of the acceptor (C–I···A, A = O, S, Se, π). The PDB IDs of the selected structures are 3DNA,[43] 4X21 [44] 5HK2 [45] and 3PP1.[46] The first one was reported in 2009 by Liu *et al.*[43] who demonstrated that the mutation of Leu99 to Ala in bacteriophage T4 lysozyme (L99A) produces an internal non-polar cavity that binds a variety of aromatic rings.[47,48] In fact this mutant lysozyme has been used to study halogen–protein interactions using halobenzenes (C_6F_5X, X = H, F, Cl, Br or I, and C_6H_5X, where X = H, CH_3 or I).[43] The authors compared the binding of the C_6H_5I ligand, which establishes a HaB with L99A, with that of benzene and toluene, which do not undergo this type of interaction. The difference in the binding energies was approximately $\Delta\Delta H$ = 0.5 kcal mol^{-1} that was attributed to the HaB. At this point it should be emphasized that this small difference can also be due to other important factors like steric effects and solvation/desolvation enthalpic contributions.

As noticed in Fig. 3a, a σ-hole is present over the tip of the I atom belonging to the PIH ligand, which confirms its ability to undergo halogen bonding interactions. This X-ray crystal struc-

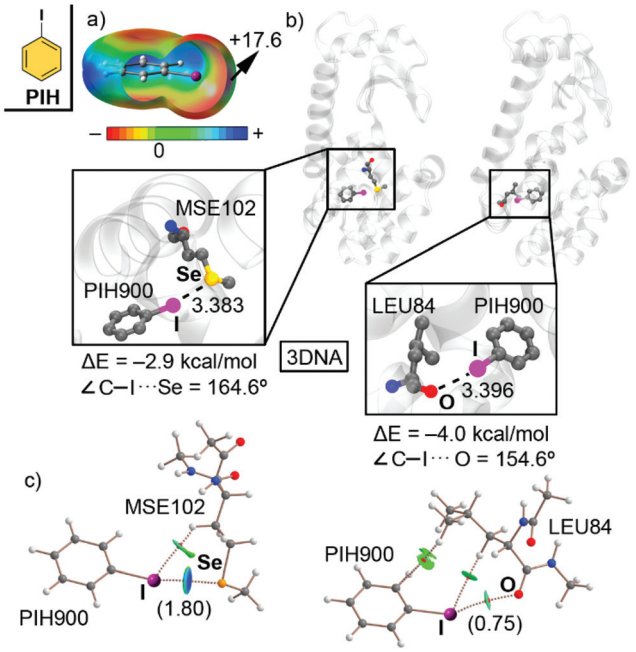

Fig. 3 (a) Open MEP surface of the PIH ligand where the blue colour is used for positive values and the red colour is used for negative values. The energy value at the iodine's σ-hole is indicated in kcal mol^{-1} (isosurface 0.001 a.u.). (b) Partial view of the X-ray crystal structure 3DNA (resolution 1.7 Å) exhibiting two HaBs, which are magnified inside the square parts of the figure (distances in Å). The HaB interaction energy value (ΔE) and C–I···Se/O angles are also indicated. (c) Distribution of intermolecular BCPs (in red) and bond paths for both HaBs. The value of the density ($10^2 \times \rho$) at the BCP defining the HaBs is also indicated in a.u. For the NCIplot, the ρ = 0.04 a.u. cut-off was used. The |RGD| isovalue used to plot the surface is 0.5 and the colour scale is −0.02 a.u. (blue) ≤ (signλ_2) ≤ 0.02 a.u. (red). In the QTAIM and NCIPlot analyses, only intermolecular interactions are represented.

ture exhibits a disorder in the position of the PIH ligand, and therefore two different HaBs can be established depending on its location (see Fig. 3b), that is, pointing to either a selenomethionine (MSE, Se as an electron donor atom) or a LEU (O as an electron donor atom) residue. The interaction energies obtained for both HaBs are −2.9 and −4.0 kcal mol^{-1}, respectively. This is likely due to the stronger Lewis base character of the O atom compared to Se, although the directionality was higher in the latter (∠C–I···Se of 164.6 degrees). These values are larger than the experimental $\Delta\Delta H$ value obtained from comparing the binding of toluene *vs.* iodobenzene (0.5 kcal mol^{-1}), thus suggesting that other factors apart from the halogen bond influence the experimental binding energy. Moreover, the H-atoms of the methyl group of toluene likely establish C–H···O/S interactions with the MSE/LEU residues since the methyl group occupies the position of the I-atom in the active center. Therefore, the $\Delta\Delta H$ value corresponds to the energetic difference between the halogen and hydrogen bonds instead of accounting only for the HaB.

In Fig. 3c the two QTAIM and NCIplot analyses are shown and it can be noticed that in both cases a bond critical point (BCP) and a bond path connects the I atom with the Se and O atoms of the MSE and LEU residues, thus characterizing the biological HaBs. In addition, ancillary HB and CH···π interactions are undertaken involving the I atom and the aromatic surface from the C_6H_5I ligand as well as the CH groups from the AA backbone. This was also confirmed in the NCIplot analysis by (i) the greenish and bluish isosurfaces located between the I and the Se/O atoms and (ii) the greenish isosurfaces placed between the CH groups from the AA backbone and the I and C atoms from the PIH ligand. The isosurface colours support the dominant role of the HaB interaction.

The PDB code 4X21 corresponds to a c-Jun N-terminal kinase 3 (JNK3) that has been recently used to exemplify the applicability of X···S halogen bonds by targeting the gatekeeper MET146.[44] The mutation of the gatekeeper residue into LEU, ALA, or THR significantly influences the selectivity and affinity of the 3WH ligand (see Fig. 4) toward JNK3. The experimental binding enthalpy of the 3WH···JNK3 complex determined by Lange *et al.*[44] was −8.3 kcal mol^{-1}, significantly stronger than that reported in the PIH···L99A complex (PDB: 3DNA).

As noticed in Fig. 4a, the 3WH ligand exhibits a region of positive electrostatic potential over the I atom, thus confirming the presence of a σ-hole. The HaB interaction involving 3WH and MET146 resulted in −1.3 kcal mol^{-1} (Fig. 4b), which represents around 16% of the total binding enthalpy measured experimentally.

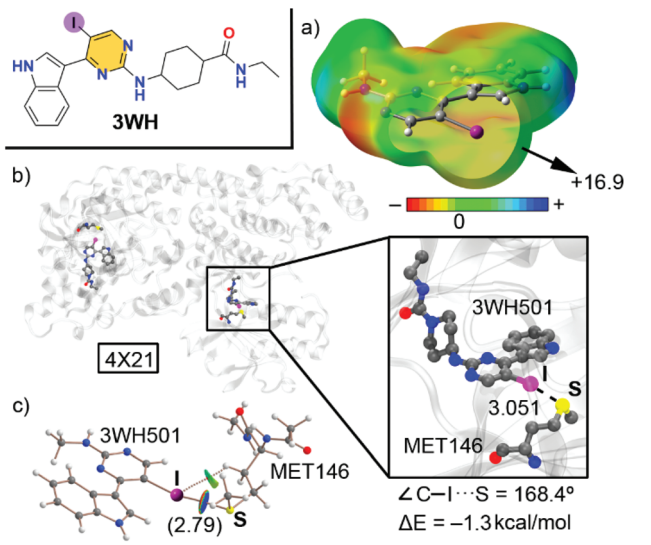

Fig. 4 (a) MEP surface (positive in blue and negative in red) of the 3WH ligand (the *N*-ethylcyclohexanecarboxamide group has been replaced by a $-CH_3$ group). The energy value at the iodine's σ-hole is given in kcal mol^{-1} (isosurface 0.001 a.u.). (b) Partial view of the X-ray crystal structure 4X21 (resolution 1.95 Å) exhibiting a HaB, which is magnified inside the square part of the figure (distances in Å). The HaB interaction energy value (ΔE) and C–I···S angle are also indicated. (c) Distribution of intermolecular BCPs (in red) and bond paths in the HaB complex. The value of the density ($10^2 \times \rho$) at the BCP defining the HaB is also indicated in a.u. For the NCIplot, the ρ = 0.04 a.u. cut-off was used. The |RGD| isovalue used to plot the surface is 0.5 and the colour scale is −0.02 a.u. (blue) ≤ (signλ_2) ≤ 0.02 a.u. (red). In the QTAIM and NCIPlot analyses, only intermolecular interactions are represented.

Finally, the QTAIM analysis (Fig. 4c) revealed the presence of a BCP and a bond path connecting the I and S atoms belonging to 3WH and MET146 moieties, respectively, thus characterizing the HaB interaction in this protein–ligand complex. In addition, an ancillary HB is characterized by the presence of a BCP and a bond path connecting the I atom of 3WH and a C–H group from MET146. This was also confirmed by the NCIplot analysis, which showed blue and green isosurfaces located between (i) the I and S atoms and (ii) the I atom from the ligand and the CH group from the AA. The NCIplot index evidences the stronger nature of the C–I···S HaB (dark blue) compared to the C–H···I (green) that dominates the complexation.

The third structure analysed herein is 5HK2 [45] that contains the human σ1 receptor complexed to the *N*-(1-benzylpiperidin-4-yl)-4-iodobenzamide ligand (61V, see Fig. 5). It is an endoplasmic-reticulum-resident transmembrane protein implicated in a variety of disorders (depression, drug addiction, *etc.*)[49,50] and it is also connected to amyotrophic lateral sclerosis.[51] The ligand binding site is buried in the centre of a cupin-like β-barrel.

In this structure, the π-system of TYR206 acts as an electron donor moiety and it should be noted that the HaB between the ligand and this residue was not commented by the original authors, likely due to the unconventional nature of the electron donor.

In Fig. 5a the MEP surface of ligand 61V shows the presence of a positive value along the C–I covalent bond, which can be attributed to the presence of a σ-hole. The interaction energy value between 61V and the TYR206 π-system resulted in −4.9 kcal mol^{-1}. Finally, AIM analysis revealed the presence of a BCP and a bond path connecting the I atom and the C atoms belonging to the aromatic surface of TYR206, thus characterizing the HaB interaction. This was further confirmed in the NCIplot analysis, which revealed the presence of a greenish isosurface positioned between the I and the aromatic system of the AA.

The last structure studied herein is 3PP1,[46] involving a new and selective MEK (mitogen-activated kinase) inhibitor with applications in cancer treatment. More precisely, the RAF (rapidly accelerated fibrosarcoma kinase)–MEK–ERK (extracellular signal-regulated kinase) pathway is implicated in the regulation of proliferative and anti-apoptotic signalling processes from growth and oncogenic factors, which are related to tumour growth, progression and metastasis.[52] Therefore, it

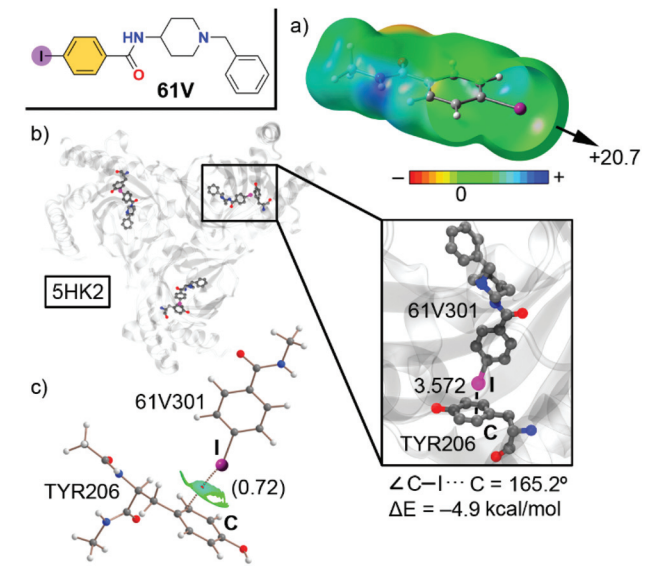

Fig. 5 (a) MEP surface (positive in blue and negative in red) of the 61V ligand (modelled as 4-iodo-*N*-methylbenzamide). The energy value at the iodine's σ-hole is given in kcal mol^{-1} (isosurface 0.001 a.u.). (b) Partial view of the X-ray crystal structure 5HK2 (resolution 3.2 Å) exhibiting a HaB, which is magnified inside the square part of the figure (distances in Å). The HaB interaction energy value (Δ*E*) and C–I···C angle are also indicated. (c) Distribution of intermolecular BCPs (in red) and bond paths in the HaB complex. The value of the density ($10^2 \times \rho$) at the BCP defining the HaB is also indicated in a.u. For the NCIplot, the ρ = 0.04 a.u. cut-off was used. The |RGD| isovalue used to plot the surface is 0.5 and the colour scale is −0.02 a.u. (blue) ≤ (signλ_2) ≤ 0.02 a.u. (red). In the QTAIM and NCIPlot analyses, only intermolecular interactions are represented.

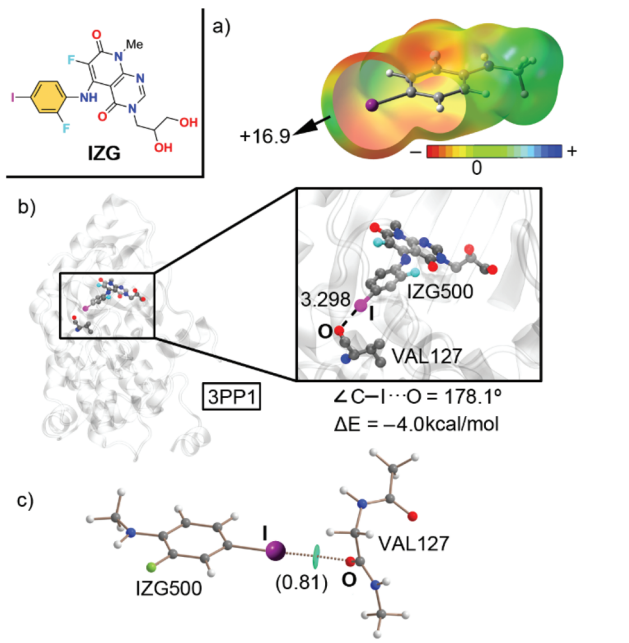

Fig. 6 (a) MEP surface (positive in blue and negative in red) of the IZG ligand (the 6-fluoro-3,8-dimethylpyrido[2,3-*d*]pyrimidine-4,7(3*H*,8*H*)-dione moiety has been replaced by a $-CH_3$ group). The energy value at the iodine's σ-hole is given in kcal mol^{-1} (isosurface 0.001 a.u.). (b) Partial view of the X-ray crystal structure 3PP1 (resolution 2.70 Å) exhibiting a HaB, which is magnified inside the square part of the figure (distances in Å). The HaB interaction energy value (Δ*E*) and C–I···O angle are also indicated. (c) Distribution of intermolecular BCPs (in red) and bond paths in the HaB complex. The value of the density ($10^2 \times \rho$) at the BCP defining the HaB is also indicated in a.u. For the NCIplot, the ρ = 0.04 a.u. cut-off was used. The |RGD| isovalue used to plot the surface is 0.5 and the colour scale is −0.02 a.u. (blue) ≤ (signλ_2) ≤ 0.02 a.u. (red). In the QTAIM and NCIPlot analyses, only intermolecular interactions are represented.

represents an interesting molecular target with a broad spectrum of therapeutic applications in cancerous and non-cancerous hyperproliferative disorders, including inflammation and immunomodulation processes.[53] Dong and collaborators synthesized a novel MEK inhibitor, named TAK-733 (IZG in Fig. 6) and structurally characterized the enzyme–inhibitor complex. This compound presents a halobenzene moiety where I and F atoms are disposed in a *meta*-substitution fashion. Interestingly, the I atom exhibits a positive potential region located on the extension of the C–I bond, thus denoting the presence of a σ-hole, which is also favored by the presence of a strong electron withdrawing group (EWG) in the vicinity, such as F. In Fig. 6b, a HaB is established between the ligand IZG and the OC carbonyl group of VAL127, a fact that passed unnoticed to the original authors. As noted, it is a highly directional HaB (C–I···O angle close to linearity) presenting an I···O distance around 3.3 Å. The computed interaction energy value resulted in −4.0 kcal mol^{-1}, in line with the results obtained for the rest of the structures.

Finally, the AIM and NCIplot analysis of this HaB complex (Fig. 6c) revealed the presence of a BCP and a bond path connecting the I and O atoms belonging to IZG and the carbonyl moiety of VAL127, respectively, thus characterizing the HaB interaction. In addition, the NCIplot analysis showed a greenish isosurface located between the I and O atoms, which served as a further confirmation of the existence and favourable nature of this biological HaB.

Conclusions

In this study, we have inspected the PDB for the analysis of HaBs in biological systems, highlighting their importance in four different protein–ligand systems. In line with previous PDB surveys existing in the literature, the carbonyl groups of VAL residues are the most abundant electron donor moieties, followed by LEU and GLY carbonyl moieties. The four selected biological HaBs, as representative cases of the four types of interactions observed, were energetically and geometrically analysed and described from a charge density perspective using QTAIM and NCIplot methodologies. Both computational tools are convenient to disclose the existence and attractive nature of biological HaBs in models of protein–ligand interactions. The QTAIM is proposed as a fourth criterion to evidence the importance of HaBs in biological systems together with the fulfilment of the other three criteria proposed in the literature.[30] We expect that the results derived from this study might be useful for those scientists working in the fields of biomolecular engineering and rational drug design.

Experimental section

PDB search

The PDB was inspected using the freely available web-based engine held by the European Bionformatics Institute (https://www.ebi.ac.uk/, accessed May 06th, 2021). All PDB structures containing iodo-organic ligands were manually scrutinized. The RNA and DNA molecules including iodinated bases were not considered as ligands. As main geometrical criteria, only HaBs exhibiting a C–I···A (A = O, S, Se and C) distance within the sum of vdW radii +0.3 Å and a C–I···A angle comprised between 160 and 180 degrees were considered. Selected hits showing protein–ligand HaBs are presented in Table S1† with an indication of the ligand ID, the electron donor residue as well as HaB distances and angles.

Theoretical methods

The calculations of the system reported herein were performed at the RI-MP2 [54] level of theory with the def2-TZVP [55] basis set using the TURBOMOLE 7.2 software. [56]Initially, the H atoms from X-ray crystal structure models (see the ESI† for cartesian coordinates) were optimized at the BP86 [57]-D3 [58]/def2-SVP [55] level of theory. These geometries were taken as starting points for single point calculations at the RI-MP2/def2-TZVP level of theory. The M33 grid has been used in the DFT calculations using TURBOMOLE. The MEP (molecular electrostatic potential) surfaces were computed at the B3LYP [59]/def2-TZVP level of theory by means of the Gaussian 16 calculation package.[60] The Bader's "atoms in molecules" theory has been used to study the interactions discussed herein by means of the AIMall calculation package.[61] The wavefunction analysis has been performed at the B3LYP/def2-TZVP level of theory. The NCIplot [62] isosurfaces correspond to both favorable and unfavorable interactions, as differentiated by the sign of the second density Hessian eigenvalue and defined by the isosurface color. The color scheme is a red-yellow-green-blue scale with red for the repulsive (ρ_{cut}^{+}) and blue for the attractive (ρ_{cut}^{-}) NCI interaction density. Yellow and green surfaces correspond to weak repulsive and weak attractive interactions, respectively.

Conflicts of interest

There are no conflicts to declare.

Acknowledgements

We acknowledge the MCIU/AEI of Spain (projects CTQ2017-85821-R and PID2020-115637GB-I00, FEDER, UE funds) for financial support.

References

1 (*a*) I. Alkorta, J. Elguero and A. Frontera, *Crystals*, 2020, **10**, 180; (*b*) A. Bauzá, I. Alkorta, J. Elguero, T. J. Mooibroek and A. Frontera, *Angew. Chem.*, 2020, **59**, 17482–17487; (*c*) A. Daolio, A. Pizzi, G. Terraneo, M. Ursini, A. Frontera and G. Resnati, *Angew. Chem.*, 2021, **60**, 14385–14389; (*d*) A. Daolio, A. Pizzi, M. Calabrese, G. Terraneo,

S. Bordignon, A. Frontera and G. Resnati, *Angew. Chem.*, 2021, **60**, DOI: 10.1002/anie.202107978.
2 A. Daolio, P. Scilabra, G. Terraneo and G. Resnati, *Coord. Chem. Rev.*, 2020, **413**, 213265.
3 Y. Xu, P. M. J. Szell, V. Kumar and D. L. Bryce, *Coord. Chem. Rev.*, 2020, **411**, 213237.
4 W. Wang, Y. Zhang and W. J. Jin, *Coord. Chem. Rev.*, 2020, **404**, 213107.
5 M. Fourmigué and A. Dhaka, *Coord. Chem. Rev.*, 2020, **403**, 213084.
6 M. S. Taylor, *Coord. Chem. Rev.*, 2020, **413**, 213270.
7 N. Biot and D. Bonifazi, *Coord. Chem. Rev.*, 2020, **413**, 213243.
8 K. T. Mahmudov, A. V. Gurbanov, V. A. Aliyeva, G. Resnati and A. J. L. Pombeiro, *Coord. Chem. Rev.*, 2020, **418**, 213381.
9 J. Pancholi and P. D. Beer, *Coord. Chem. Rev.*, 2020, **416**, 213281.
10 G. Resnati and P. Metrangolo, *Coord. Chem. Rev.*, 2020, **420**, 213409.
11 D. von der Heiden, A. Vanderkooy and M. Erdélyi, *Coord. Chem. Rev.*, 2020, **407**, 213147.
12 P. C. Ho, J. Z. Wang, F. Meloni and I. Vargas-Baca, *Coord. Chem. Rev.*, 2020, **422**, 213464.
13 S. Scheiner, M. Michalczyk and W. Zierkiewicz, *Coord. Chem. Rev.*, 2020, **405**, 213136.
14 A. Bauzá and A. Frontera, *Coord. Chem. Rev.*, 2020, **404**, 213112.
15 A. Bauzá, S. K. Seth and A. Frontera, *Coord. Chem. Rev.*, 2019, **384**, 107–125.
16 *Hydrogen Bonded Supramolecular Materials*, ed. Z.-T. Li and L.-Z. Wu, Springer-Verlag, Berlin, 2015.
17 G. A. Jeffrey and W. Saenger, *Hydrogen Bonding in Biological Structures*, Springer-Verlag, Berlin, 1991.
18 Y. Marechal, *The Hydrogen Bond and the Water Molecule: The Physics and Chemistry of Water*, Aqueous and Bio-Media, Elsevier Science, 2006.
19 W. Wu, M. K. Samoszuk, S. A. A. Comhair, M. J. Thomassen, C. F. Farver, R. A. Dweik, M. S. Kavuru, S. C. Erzurum and S. L. Hazen, *J. Clin. Invest.*, 2000, **105**, 1455–1463.
20 J. M. Vargason, B. F. Eichman and P. S. Ho, *Nat. Struct. Biol.*, 2000, **7**, 758–761.
21 A. Sassa, Y. Kanemaru, N. Kamoshita, M. Honma and M. Yasui, *Genes Environ.*, 2016, **38**, 17.
22 P. S. Ho and D. M. Anderson, in *Halogen Bonding in Solution*, ed. S. Huber, Wiley-VCH Verlag GmbH & Co, Weinheim, Germany, 2021, pp. 335–362.
23 A. Bachi, I. Dalle-Donne and A. Scaloni, *Chem. Rev.*, 2013, **113**, 596–698.
24 E. Fernández, *Aust. J. Clin. Neurol.*, 2015, **2**, 1088.
25 P. S. Ho, *Future Med. Chem.*, 2017, **9**, 637–640.
26 P. S. Ho, *Top. Curr. Chem.*, 2015, **358**, 241–276.
27 M. C. Ford and P. S. Ho, *J. Med. Chem.*, 2016, **59**, 1655–1670.
28 P. Auffinger, F. A. Hays, E. Westhof and P. S. Ho, *Proc. Natl. Acad. Sci. U. S. A.*, 2004, **101**, 16789–16794.
29 M. R. Scholfield, C. M. Zanden, M. Carter and P. S. Ho, *Protein Sci.*, 2013, **22**, 139–152.
30 R. S. Czarny, A. N. Ho and P. S. Ho, *Chem. Rec.*, 2021, **21**, 1240–1251.
31 M. A. A. Ibrahim, *J. Comput. Chem.*, 2011, **32**, 2564–2574.
32 M. Kolar and P. Hobza, *J. Chem. Theory Comput.*, 2012, **8**, 1325–1333.
33 M. Kolar, P. Hobza and A. K. Bronowska, *Chem. Commun.*, 2013, **49**, 981–983.
34 M. Carter, A. K. Rappe and P. S. Ho, *J. Chem. Theory Comput.*, 2012, **8**, 2461–2473.
35 A. Frontera and A. Bauzá, *J. Chem. Theory Comput.*, 2020, **16**, 4744–4752.
36 M. N. Piña, A. Frontera and A. Bauzá, *ACS Chem. Biol.*, 2020, **15**, 1942–1948.
37 R. F. W. Bader, *Chem. Rev.*, 1991, **91**, 893–928.
38 G. R. Desiraju, P. S. Ho, L. Kloo, A. C. Legon, R. Marquardt, P. Metrangolo, P. Politzer, G. Resnati and K. Rissanen, *Pure Appl. Chem.*, 2013, **85**, 1711–1713.
39 H. M. Berman, J. Westbrook, Z. Feng, G. Gilliland, T. N. Bhat, H. Weissig, I. N. Shindyalov and P. E. Bourne, *Nucleic Acids Res.*, 2000, **28**, 235–242.
40 E. R. Johnson, S. Keinan, P. Mori-Sanchez, J. Contreras-Garcia, A. J. Cohen and W. Yang, *J. Am. Chem. Soc.*, 2010, **132**, 6498–6506.
41 (*a*) S. Sirimulla, J. B. Bailey, R. Vegesna and M. Narayan, *J. Chem. Inf. Model.*, 2013, **53**, 2781–2791; (*b*) Z. Xu, Z. Yang, Y. Liu, Y. Lu, K. Chen and W. Zhu, *J. Chem. Inf. Model.*, 2014, **54**, 69–78; (*c*) Q. Zhang, Z. Xu and W. Zhu, *J. Chem. Inf. Model.*, 2017, **57**, 22–26; (*d*) Q. Zhang, Z. Xu, J. Shi and W. Zhu, *J. Chem. Inf. Model.*, 2017, **57**, 1529–1534; (*e*) R. Ferreira de Freitas and M. Schapira, *MedChemCommun*, 2017, **8**, 1970–1981; (*f*) L. A. Hardegger, B. Kuhn, B. Spinnler, L. Anselm, R. Ecabert, M. Stihle, B. Gsell, R. Thoma, J. Diez, J. Benz, J.-M. Plancher, G. Hartmann, D. W. Banner, W. Haap and F. Diederich, *Angew. Chem., Int. Ed.*, 2011, **50**, 314–318.
42 (*a*) A. Tosstorff, J. Cole, R. Taylor, S. F. Harris and B. Kuhn, *J. Chem. Inf. Model.*, 2020, **60**, 6595–6611; (*b*) N. K. Shinada, A. G. de Brevern and P. Schmidtke, *J. Med. Chem.*, 2019, **62**(21), 9341–9356; (*c*) B. Kuhn, E. Gilberg, R. Taylor, J. Cole and O. Korb, *J. Med. Chem.*, 2019, **62**, 10441–10455.
43 L. Liu, W. A. Baase and B. W. Matthews, *J. Mol. Biol.*, 2009, **385**, 595–605.
44 A. Lange, M. Gunther, F. M. Buttner, M. O. Zimmermann, J. Heidrich, S. Hennig, S. Zahn, C. Schall, A. Sievers-Engler, F. Ansideri, P. Koch, M. Laemmerhofer, T. Stehle, S. A. Laufer and F. M. Boeckler, *J. Am. Chem. Soc.*, 2015, **137**, 14640–14652.
45 H. R. Schmidt, S. Zheng, E. Gurpinar, A. Koehl, A. Manglik and A. C. Kruse, *Nature*, 2016, **532**, 527–530.
46 Q. Dong, D. R. Dougan, X. Gong, P. Halkowycz, B. Jin, T. Kanouni, S. M. O'Connell, N. Scorah, L. Shi, M. B. Wallace and F. Zhou, *Bioorg. Med. Chem. Lett.*, 2011, **21**, 1315–1319.

47 A. E. Eriksson, W. A. Baase, X.-J. Zhang, D. W. Heinz, M. Blaber, E. P. Baldwin and B. W. Matthews, *Science*, 1992, **255**, 178–183.
48 A. E. Eriksson, W. A. Baase, J. A. Wozniak and B. W. Matthews, *Nature*, 1992, **355**, 371–373.
49 T. P. Su, T. Hayashi, T. Maurice, S. Buch and A. E. Ruoho, *Trends Pharmacol. Sci.*, 2010, **31**, 557–566.
50 T. A. Mavlyutov, M. L. Epstein, Y. I. Verbny, M. S. Huerta, I. Zaitoun, L. Ziskind-Conhaim and A. E. Ruoho, *Neuroscience*, 2013, **240**, 129–134.
51 A. Al-Saif, F. Al-Mohanna and S. Bohlega, *Ann. Neurol.*, 2011, **70**, 913–919.
52 (*a*) R. Seger and E. C. Krebs, *FASEB J.*, 1995, **9**, 726; (*b*) O. K. Mirzoeva, D. Das, L. M. Heiser, S. Bhattacharya, D. Siwak, R. Gendelman, N. Bayani, N. J. Wang, R. M. Neve, Y. Guan, Z. Hu, Z. Knight, H. S. Feiler, P. Gascard, B. Parvin, P. T. Spellman, K. M. Shokat, A. J. Wyrobek, M. J. Bissell, F. McCormick, W.-L. Kuo, G. B. Mills, J. W. Gray and W. M. Korn, *Cancer Res.*, 2009, **69**, 565.
53 (*a*) R. Herrera and J. S. Sebolt-Leopold, *Trends Mol. Med.*, 2002, **8**, S27; (*b*) C. Montagut and J. Settleman, *Cancer Lett.*, 2009, **283**, 125; (*c*) M. J. Thiel, C. J. Schaefer, M. E. Lesch, J. L. Mobley, D. T. Dudley, H. Tecle, S. D. Barrett, D. J. Schrier and C. M. Flory, *Arthritis Rheum.*, 2007, **56**, 3347.
54 F. Weigend and M. Häser, *Theor. Chem. Acc.*, 1997, **97**, 331–340.
55 F. Weigend and R. Ahlrichs, *Phys. Chem. Chem. Phys.*, 2005, **7**, 3297–3305.
56 S. G. Balasubramani, *et al.*, *J. Chem. Phys.*, 2020, **152**, 184107.
57 A. D. Becke, *Phys. Rev. A: At., Mol., Opt. Phys.*, 1988, **38**, 3098–3100.
58 S. Grimme, J. Antony, S. Ehrlich and H. Krieg, *J. Chem. Phys.*, 2010, **132**, 154104.
59 (*a*) A. D. Becke, *J. Chem. Phys.*, 1993, **98**, 5648–5652; (*b*) P. J. Stephens, F. J. Devlin, C. F. Chabalowski and M. J. Frisch, *J. Phys. Chem.*, 1994, **98**, 11623–11627.
60 M. J. Frisch, G. W. Trucks, H. B. Schlegel, G. E. Scuseria, M. A. Robb, J. R. Cheeseman, G. Scalmani, V. Barone, G. A. Petersson, H. Nakatsuji, X. Li, M. Caricato, A. V. Marenich, J. Bloino, B. G. Janesko, R. Gomperts, B. Mennucci, H. P. Hratchian, J. V. Ortiz, A. F. Izmaylov, J. L. Sonnenberg, D. Williams-Young, F. Ding, F. Lipparini, F. Egidi, J. Goings, B. Peng, A. Petrone, T. Henderson, D. Ranasinghe, V. G. Zakrzewski, J. Gao, N. Rega, G. Zheng, W. Liang, M. Hada, M. Ehara, K. Toyota, R. Fukuda, J. Hasegawa, M. Ishida, T. Nakajima, Y. Honda, O. Kitao, H. Nakai, T. Vreven, K. Throssell, J. A. Montgomery Jr., J. E. Peralta, F. Ogliaro, M. J. Bearpark, J. J. Heyd, E. N. Brothers, K. N. Kudin, V. N. Staroverov, T. A. Keith, R. Kobayashi, J. Normand, K. Raghavachari, A. P. Rendell, J. C. Burant, S. S. Iyengar, J. Tomasi, M. Cossi, J. M. Millam, M. Klene, C. Adamo, R. Cammi, J. W. Ochterski, R. L. Martin, K. Morokuma, O. Farkas, J. B. Foresman and D. J. Fox, *Gaussian 16, Revision A.01*, Gaussian, Inc., Wallingford CT, 2016.
61 T. A. Keith, *TK Gristmill Software, AIMAll (Version 19.10.12)*, Overland Park KS, USA, 2019 (aim.tkgristmill.com).
62 J. Contreras-García, E. R. Johnson, S. Keinan, R. Chaudret, J.-P. Piquemal, D. N. Beratan and W. Yang, *J. Chem. Theory Comput.*, 2011, **7**, 625–632.